inorganics

MDPI

Article

Synthesis of K^+ and Na^+ Synthetic Sodalite Phases by Low-Temperature Alkali Fusion of Kaolinite for Effective Remediation of Phosphate Ions: The Impact of the Alkali Ions and Realistic Studies

Stefano Bellucci [1,*], Mohamed Hamdy Eid [2,3], Ilona Fekete [4], Szűcs Péter [3], Attila Kovács [3], Sarah I. Othman [5], Jamaan S. Ajarem [6], Ahmed A. Allam [7] and Mostafa R. Abukhadra [2,8,*]

1 INFN-Laboratori Nazionali di Frascati, Via. E. Fermi 54, 00044 Frascati, Italy
2 Geology Department, Faculty of Science, Beni-Suef University, Beni-Suef 65211, Egypt
3 Institute of Environmental Management, Faculty of Earth Science, University of Miskolc, 3515 Miskolc-Egyetemváros, Hungary
4 Department of Environmental Analysis and Environmental Technology, Institute of Environmental Science, Hungarian University of Agriculture and Life Science, 1118 Budapest, Hungary
5 Biology Department, College of Science, Princess Nourah Bint Abdulrahman University, Riyadh 11564, Saudi Arabia
6 Zoology Department, College of Science, King Saud University, Riyadh 11451, Saudi Arabia
7 Zoology Department, Faculty of Science, Beni-Suef University, Beni-Suef 65211, Egypt
8 Materials Technologies and Their Applications Lab, Geology Department, Faculty of Science, Beni-Suef University, Beni-Suef 65211, Egypt
* Correspondence: stefano.bellucci@lnf.infn.it (S.B.); Abukhadra89@science.bsu.edu.eg (M.R.A.)

Abstract: Two sodalite phases (potassium sodalite (K.SD) and sodium sodalite (Na.SD)) were prepared using alkali fusion of kaolinite followed by a hydrothermal treatment step for 4 h at 90 °C. The synthetic phases were characterized as potential adsorbents for PO_4^{3-} from the aqueous solutions and real water from the Rákos stream (0.52 mg/L) taking into consideration the impact of the structural alkali ions (K^+ and Na^+). The synthetic Na.SD phase exhibited enhanced surface area (232.4 m^2/g) and ion-exchange capacity (126.4 meq/100 g) as compared to the K.SD phase. Moreover, the Na.SD phase exhibited higher PO_4^{3-} sequestration capacity (Q_{max} = 261.6 mg g^{-1} and Q_{sat} = 175.3 mg g^{-1}) than K.SD phase (Q_{max} = 201.9 mg g^{-1} and Q_{sat} = 127.4 mg g^{-1}). The PO_4^{3-} sequestration processes of both Na.SD and K.SD are spontaneous, homogenous, and exothermic reactions that follow the Langmuir isotherm and pseudo-first-order kinetics. Estimation of the occupied active site density validates the enrichment of the Na.SD phase with high quantities of active sites (Nm = 86.1 mg g^{-1}) as compared to K.SD particles (Nm = 44.4 mg g^{-1}). Moreover, the sequestration and Gaussian energies validate the cooperation of physisorption and weak chemisorption processes including zeolitic ion exchange reactions. Both Na.SD and K.SD exhibit significant selectivity for PO_4^{3-} in the coexisting of other common anions (Cl^-, SO_4^{2-}, HCO_3^-, and NO_3^-) and strong stability properties. Their realistic application results in the complete adsorption of PO_4^{3-} from Rákos stream water after 20 min (Na. SD) and 60 min (K.SD).

Keywords: sodalite; zeolite; phosphate; adsorption; equilibrium; Rákos stream

check for updates

Citation: Bellucci, S.; Eid, M.H.; Fekete, I.; Péter, S.; Kovács, A.; Othman, S.I.; Ajarem, J.S.; Allam, A.A.; Abukhadra, M.R. Synthesis of K^+ and Na^+ Synthetic Sodalite Phases by Low-Temperature Alkali Fusion of Kaolinite for Effective Remediation of Phosphate Ions: The Impact of the Alkali Ions and Realistic Studies. *Inorganics* **2023**, *11*, 14. https://doi.org/10.3390/inorganics11010014

Academic Editor: Carlos Martínez-Boubeta

Received: 25 October 2022
Revised: 10 December 2022
Accepted: 12 December 2022
Published: 27 December 2022

Copyright: © 2023 by the authors. Licensee MDPI, Basel, Switzerland. This article is an open access article distributed under the terms and conditions of the Creative Commons Attribution (CC BY) license (https://creativecommons.org/licenses/by/4.0/).

1. Introduction

During recent decades, the wide detection of the eutrophication phenomena in several lakes and water bodies has represented a critical environmental issue that negatively affects the balance of the aquatic ecosystem as well as aquatic organisms [1,2]. This phenomenon is associated with the extensive and random growth of microorganisms, algae, and phytoplankton causing depletion in oxygen content as well as water quality [3,4]. This phenomenon is related mainly to the continuous and uncontrolled discharge of sewage

water, agricultural drainage water, and industrial wastewater into freshwater bodies with their overloads on phosphorous and nitrogen-bearing compounds, which are essential nutrients [5,6]. This is a worldwide problem and was detected in several localities in Europe, such as in Hungary. The most frequent water quality issue in Hungary in terms of surface water is that concerning nutrient loading and external organic matter [7].

Phosphorous and its phosphate compounds are common chemicals and raw materials of extensive application in numerous industries such as in fertilizers, detergents, and metal coating [5,8]. The existence of phosphate in aquatic environments as a nutrient is vital for aquatic organisms; however, a high concentration above 0.05 mg/L accelerates eutrophication effects and depletion of the dissolved oxygen and causes some health side effects (osteoporosis and heart damage) [3,4,9]. Discharged industrial and municipal wastewater is an essential source of phosphate in addition to having a significant effect on agricultural run-off and mining activities [2,10,11]. Previous studies demonstrate the existence of phosphate at 4 to 15 mg/L concentration within municipal wastewater and 14 to 25 mg/L in the effluents of some chemical industries, such as detergent and metal coating [10]. Dissolved phosphate ions normally exhibit ionic species and are controlled essentially by pH (H_3PO_4 (pH < 2), $H_2PO_4^-$ (pH 3–7), HPO_4^{2-} (pH 7–11), and PO_4^{3-} (pH > 12)) [4]. Based on the dissociation constant (pKa) of H_3PO_4, the PO_4^{3-} form is less dominant as compared to the monovalent and divalent forms in wastewaters [4].

Therefore, preserving the phosphate concentration in discharged effluents at the recommended limit is a significant environmental and technical challenge in recent years. Different types of physical, chemical, and biological techniques have been assessed for their effectiveness in reaching this target, including biological treatment, chemical precipitation, catalytic wet-air oxidation, ion exchange, and adsorption [12–14]. The adsorption reduction of phosphate was reported and recommended in several studies as a highly effective, low-cost, and simple technique [12,15,16]. The selection and fabrication of the adsorbent materials depend strongly on the availability of their raw materials, the simplicity of the preparation procedures, the fabrication cost, adsorption kinetics, recyclability value, selectivity properties, biodegradability, and high uptake capacity [17,18]. Among the studied adsorbents of phosphate, Ca/mesoporous silica [19], MOFs [20], Mg/Al modified biochar [5], biochar-modified zeolite [16], Biochar [21], alginate@ZnFe-LDHs [14], ZIF-8/hydroxylated MWCNT [22], and Ca/Fe LDHs [23] were reported as effective and promising materials.

The natural and synthetic aluminosilicate structures, especially the zeolite phases, were identified as promising low-cost and effective adsorbents during the adsorption of phosphate ions [23,24]. Synthetic zeolite adsorbents are characterized by highly ordered nanoporous structure, significant surface area, non-toxicity, ion-exchange capacity, mechanical stability, structural flexibility, and surface reactivity [25–27]. Generally, zeolite is a microporous, crystalline, and hydrated aluminosilicate material of alkaline and/or alkaline earth ions. Its structure involves corner oxygen shared three-dimensional SiO_4 and Al_2O_4 tetrahedral units and their linking together to form a series of connected cages with numerous nanopores [28–30]. The structure of zeolite commonly exhibits negative charges as a result of the common isomorphic substitution processes between the silicon and aluminum ions [30,31]. These negative charges on the crystal lattice of zeolite can be neutralized by the exchangeable cations within its structural pores, which are normally sodium or potassium ions. Therefore, the quantities of such ions are the controlling factor during the estimation of the ion-exchange capacity of zeolite and significantly affect its efficiency during the removal of the dissolved ions [4].

However, most of the synthetic zeolite phases, such as zeolite-A, sodalite, cancrinite, zeolite-P, zeolite-Y, and zeolite-X, were studied extensively as adsorbents and ion exchangers for the effective decontamination of numerous pollutants, other synthetic phases have not yet been covered by sufficient studies, especially their modified forms [25,32–34]. Moreover, it was reported that the morphology and physicochemical properties of the synthetic phases of zeolite, such as porosity, surface area, crystalline degree, ion-exchange capacity,

and adsorption affinity, depend strongly on the starting raw materials as well as the applied synthesis conditions, including the procedures, temperature, time interval, and the used alkaline solution [27,35]. In the later periods, alkali fusion methods during the preparation of zeolite were recommended to obtain a more stable form of zeolite with enhanced crystallinity and ion-exchange capacity [36].

Therefore, the present study involved the synthesis of two sodalite phases (sodium sodalite and potassium sodalite) from natural Egyptian kaolinite as new forms of synthetic zeolite and potential adsorbents of phosphate ions from the aqueous solutions and realistic polluted water. The impact of the incorporated alkali metal ions (K^+ and Na^+) in the sodalite structure on its adsorption properties was assessed based on the effect of the different experimental variables as well as the classic equilibrium investigation and the advanced isotherm modeling based on the statistical physics theory and the associated steric and energetic parameters. This was followed by the realistic sequestration of phosphate ions from the Rákos stream, Northern Budapest, Hungary, considering the obtained best conditions.

2. Experimental Work

2.1. The Studied Area and Sampling

2.1.1. Location of Rákos Stream

The Rákos stream is located in the northern part of Budapest and is one of the tributaries of the Danube River. The total length of the watercourse is approximately 44 km, covering an area of about 185 km^2 (Figure 1). The Rákos stream originates in the area between Gödöllő and Szada and flows southwards through the town of Gödöllő, then inland to Isaszeg and Pécel, and falls into the Danube to the north of Budapest. The Rákos stream comes from several branches at the foot of the 345 m high Margita Hill and none of these branches has a source of high water yield. The eastern branch, which is considered to be the main branch, emerges at the administrative boundary of Gödöllő and Szada as a diffuse bed source, which was later incorporated into a swimming pool (Blaha Lujza bath in Gödöllő). The western branch (Kis-Rákos stream) emerges at Erzsébet Park in Gödöllő. The 12 lakes between Gödöllő and Isaszeg testify to the former peat mining that occurred there. The properties of the Rákos stream show that a water catchment area's overall ecological status is strongly affected by human activity, which is defined by hydromorphological changes and sources of chemical pollution [37]. The significant impact of human activity on the Rákos stream is expressed in its high concentrations of chloride, phosphate, ammonium, nitrate ions, and COD [37].

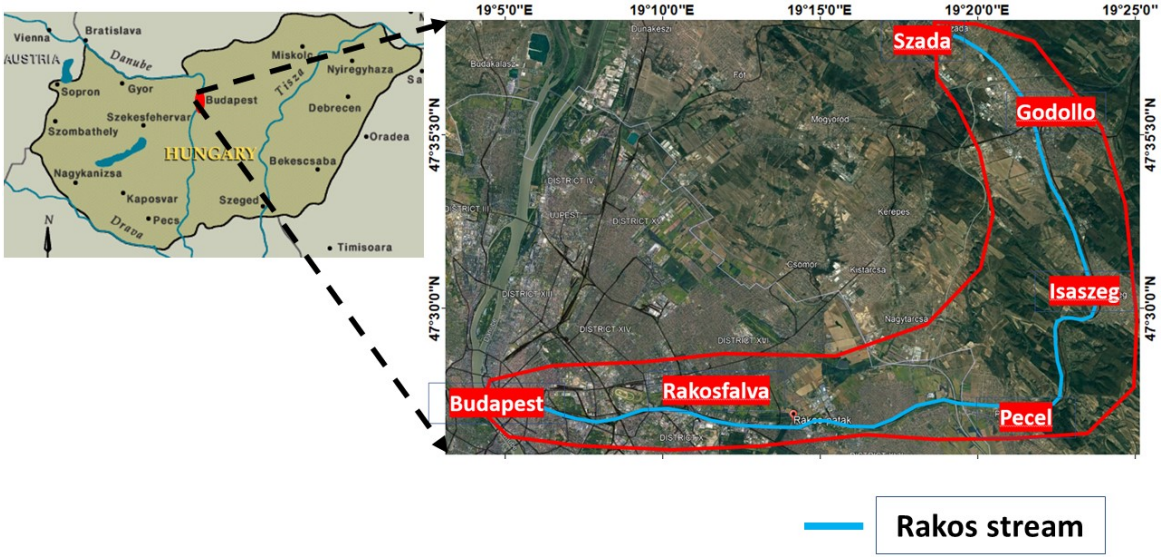

Figure 1. Location map of the studied Rákos stream and positions of the collected water samples.

2.1.2. The Water Sampling and Phosphate Content

The samples were collected in February from 13 points along the Rákos stream, as presented in Figure 1. The sampling points included the first two points in Budapest, point 3 in Pécel, point 4 between Pécel and Isaszeg, and two points in Gödöllő near the source of the Rákos stream. The samples were collected from these locations to include different kinds of land uses, such as agricultural land, urban area, forested area, water treatment plant, and industrial areas, which might be potential sources of pollution (ammonia, chloride, sulfate, nitrate, and phosphate). The water samples were collected in 1.5l polyethylene bottles after washing them carefully 3 times with water from the Rákos stream. The collected samples were transported immediately to the laboratory for analysis to avoid the growth of microorganisms (biological reaction) which can change the state of constituents and also the concentration of reliable analytical results. The samples were preserved in a refrigerator at 4 °C during the analysis period. The determined PO_4^{3-} concentrations in the collected samples demonstrated that the saturation of sample 5 (Isaszeg) had the highest concentration (528.355 mg m^{-3} (0.52 mg L^{-1})) (Table S1). This point is located between artificial surfaces and forested and semi-natural areas. According to European standards, the PO_4^{3-} concentration in low-land streams should not exceed 200 mg m^{-3} (0.2 mg L^{-1}); therefore, the water at point 5 was highly polluted with phosphate ions.

2.2. Materials

Used kaolinite as a precursor during the production of the sodalite phases was obtained as a ground product from the Central Metallurgical Research & Development Institute, Egypt, after primarily refining the steps. Sodium hydroxide (NaOH) (97%; Alfa Aesar; Egypt) and potassium hydroxide (KOH) pellets (90%; Sigma-Aldrich; Egypt) were applied during the hydrothermal production of sodalite. Phosphate standard solution (1000 mg L^{-1}) was used during the preparation of the polluted aqueous solutions at different concentrations during the adsorption experiments.

2.3. Synthesis of Sodalite

The synthesis of the sodalite phases was performed by alkali fusion followed by hydrothermal treatment processes. The kaolinite powder was mixed homogenously with the NaOH and KOH pellets at a weight ratio of 1 (kaolinite): 2 (alkali hydroxide) as separated tests and fused for 4 h at 200 °C. The obtained kaolinite/alkalis fused products were ground to be within the size range of 25 μm to 100 μm and 6 g of each product was dispersed within 100 mL of distilled water under stirring for 120 min at 70 °C. After that, the resulting mixtures or slurries were transferred into two autoclaves of Teflon lined with stainless steel and treated for 4 h at 90 °C. The formed solid phases were extracted using centrifugation and then the products of the two systems were washed several times and neutralized using distilled water. Finally, the two products were dried overnight at 85 °C, kept in specific containers, and labeled as Na.SD (sodium sodalite) and K.SD (potassium sodalite).

2.4. Characterization Techniques

The crystalline transformation of kaolinite into zeolite was followed based on the resulting XRD patterns using an X-ray diffractometer (PANalytical (Empyrean)) within a determination scanning range of 5° to 70°. Furthermore, the associated changes in the chemical functional groups during the fabrication of the sodalite phases were inspected based on their FT-IR spectra utilizing a Fourier-transform infrared spectrometer (Shimadzu FTIR−8400S) within the determination frequency range of 400 cm^{-1} to 4000 cm^{-1}. The morphologies of Na.SD, as well as K.SD, were described based on their SEM images using a scanning electron microscope (Gemini, Zeiss-Ultra 55) with 30 kV as the accelerating voltage. The surface areas as well as the porosity of both Na.SD and K.SD were measured using a Beckman Coulter surface area analyzer (type SA 3100) through consideration of the resulting nitrogen isotherm curves of the two products. The zeta potential values were

measured using a zetasizer attached to a zeta cell (Malvern, version 7.11) at different pH and the results were applied to determine the pH value at zero-point charge (pH (ZPC)).

2.5. Batch Adsorption of PO_4^{3-} from Aqueous Solutions and Real Water

The adsorption of PO_4^{3-} by the two phases of sodalite was accomplished in triplicate batch form considering the essential experimental variables such as the solutions' pH (pH 2 to 8), sodalite dosages (0.1 g L^{-1} to 0.5 g L^{-1}), contact time (30 min to 960 min), temperature (20 °C to 50 °C), and PO_4^{3-} concentrations (50 to 350 mg L^{-1}) considering the treated volume at a fixed value of 100 mL. By the end of each test, the concentrations of the rest PO_4^{3-} ions were determined using a Dionex DX-120 ion chromatography device. The measured concentrations of PO_4^{3-} (Ce) were used to obtain the adsorption capacities (Qe) of Na.SD and K.SD according to Equation (1) considering the tested volume (mL), the starting concentration (mg L^{-1}), and sodalite dosages (mg). All the adsorption tests were conducted in triplicate forms and the presented results in all the inserted graphs are in their average values.

$$Q_{e\ (mg/g)} = \frac{(C_o - C_e)V}{m} \quad (1)$$

At the end of the batch adsorption studies of PO_4^{3-} from the aqueous solutions, the materials will be applied in the adsorption of phosphate ions from the water of the Rákos stream based on the experimentally detected best conditions.

2.6. Kinetic and Isotherm Studies

The sequestration systems of PO_4^{3-} were illustrated based on the theoretical assumptions of different classic kinetic (pseudo-first-order and pseudo-second-order models), traditional isotherm (Langmuir, Freundlich, and Dubinin–Radushkevich models), and advanced isotherm models (monolayer model of one energy site) according to statistical physics theory (Table 1). This was inspected based on the non-linear fitting results of the PO_4^{3-} sequestration results, with the equations of these models considering the observed values of the determination coefficient (R^2) (Equation (2)) and chi-squared (χ^2) (Equation (3)). Regarding the non-linear fitting degrees of the PO_4^{3-} sequestration results with the different equations of the advanced equilibrium models based on statistical physics theory, these were considered according to the determination coefficient values (R^2) and the recognized root mean square error (RMSE) (Equation (4)). The m', p, Qi_{cal}, and Qi_{exp} symbols in Equation (4) signify the sequestration data, sequestration parameters, theoretical sequestration capacity of PO_4^{3-}, and the experimentally determined sequestration capacity, respectively.

$$R^2 = 1 - \frac{\sum (Q_{e,\ exp} - Q_{e,\ cal})^2}{\sum (Q_{e,\ exp} - Q_{e,\ mean})^2} \quad (2)$$

$$X^2 = \sum \frac{(Q_{e,\ exp} - Q_{e,\ cal})^2}{Q_{e,\ cal}} \quad (3)$$

$$RMSE = \sqrt{\frac{\sum_{i=1}^{m} (Qi_{cal} - Qi_{exp})^2}{m' - p}} \quad (4)$$

Table 1. Nonlinear equations of kinetic, classic isotherm, and advanced isotherm models.

Kinetic Models		
Model	**Equation**	**Parameters**
Pseudo-first-order	$Q_t = Q_e\left(1 - e^{-k_1 \cdot t}\right)$	Q_t (mg g^{-1}) is the adsorbed ions at time (t), and K_1 is the rate constant of the first-order adsorption (1 min^{-1})
Pseudo-second-order	$Q_t = \frac{Q_e^2\, k_2 t}{1 + Q_e k_2 t}$	Q_e is the quantity of adsorbed ions after equilibration (mg g^{-1}), and K_2 is the model rate constant (g mg^{-1} min^{-1}).
Classic Isotherm Models		
Model	**Equation**	**Parameters**
Langmuir	$Q_e = \frac{Q_{max}\, bC_e}{(1 + bC_e)}$	C_e is the rest ions concentration (mg L^{-1}), Q_{max} is the theoritical maximum adsorption capacity (mg g^{-1}), and b is the Langmuir constant (L mg^{-1})
Freundlich	$Q_e = K_f C_e^{1/n}$	K_F (mg g^{-1}) is the constant of Freundlich model related to the adsorption capacity and n is the constant of Freundlich model related to the adsorption intensities
Dubinin–Radushkevich	$Q_e = Q_m e^{-\beta \varepsilon^2}$	β (mol^2 KJ^{-2}) is the D–R constant, ε (KJ^2 mol^{-2}) is the polanyil potential, and Q_m is the adsorption capacity (mg/g)
Advanced Isotherm Models		
Model	**Equation**	**Parameters**
Monolayer model with one energy site (Model 1)	$Q = nN_o = \frac{nN_M}{1 + \left(\frac{C1/2}{C}\right)^n} = \frac{Q_o}{1 + \left(\frac{C1/2}{C}\right)^n}$	Q is the adsorbed quantities in mg g^{-1} n is the number of adsorbed ions per site Nm is the density of the effective receptor sites (mg g^{-1}) Q_o is the adsorption capacity at the saturation state in mg g^{-1} C1/2 is the concentration of the ions at half saturation stage in mg L^{-1} C1 and C2 are the concentrations of the ions at the half saturation stage for the first active sites and the second active sites, respectively n1 and n2 are the adsorbed ions per site for the first active sites and the second active sites, respectively
Monolayer model with two energy sites (Model 2)	$Q = \frac{n_1 N_{1M}}{1 + \left(\frac{C_1}{C}\right)^{n_1}} + \frac{n_2 N_{2M}}{1 + \left(\frac{C_2}{C}\right)^{n_2}}$	
Double layer model with one energy site (Model 3)	$Q = Q_o \frac{\left(\frac{C}{C1/2}\right)^n + 2\left(\frac{C}{C1/2}\right)^{2n}}{1 + \left(\frac{C}{C1/2}\right)^n + \left(\frac{C}{C1/2}\right)^{2n}}$	
Double layer model with two energy sites (Model 3)	$Q = Q_o \frac{\left(\frac{C}{C1}\right)^n + 2\left(\frac{C}{C2}\right)^{2n}}{1 + \left(\frac{C}{C1}\right)^n + \left(\frac{C}{C2}\right)^{2n}}$	

3. Results and Discussion

3.1. Characterization of the Sodalite Adsorbents

The obtained XRD pattern of kaolinite as well as the formed structures reflected the successful conversion of kaolinite into sodalite phases by the alkali fusion method followed by hydrothermal treatment by NaOH or KOH. The used kaolinite, as a highly crystalline mineral, confirmed the dominant phases through the identified peaks at 12.3° (001), 24.9° (002), and 26.6° (111) (Figure 2A) (XRD. No. 04-012-5104) (Figure 2A). The synthetic zeolite phases, either of NaOH or KOH, exhibit the identified peak of sodalite zeolite (ref. code: 04-009-5259) (Figure 2A). The recognized peaks of Na-sodalite (Na.SD) are 14.33° (110), 24.69° (221), 31.84° (310), 35° (222), 38.2° (321), and 43.09° (330) (ref. code: 04-009-5259) (Figure 2A). The detected peaks of K-sodalite (K.SD) are 14.48° (110), 24.76° (221), 31.98° (310), 35.09° (222), 38.44° (321), and 43.22° (330) (ref. code: 04-009-5259) (Figure 2A). The remarkable deviation in the positions of the diffraction peaks of K-sodalite as compared to Na-sodalite demonstrate the structural effects of the incorporated ions considering the differences in the ionic radius (1.94 Å (sodium) and 1.34 Å (potassium)) and substitution capacity.

The morphological studies also confirmed the strong conversion of the flaky and layered grains of raw kaolinite, with its pseudo-hexagonal shapes (Figure S1), into different forms (Figure 2B,C). While the synthetic Na.SD particles appeared as remarkable and commonly separated spherical grains (Figure 2B), the synthetic K.SD particles exhibited a commonly agglomerated shape of spherical to cubic grains (Figure 2C) which strongly affected their textural properties (Table 2). The measured BET surface areas of K.SD and Na.SD were 217.6 m^2 g^{-1} and 232.4 m^2 g^{-1}, respectively. Additionally, the Na.SD phase exhibited a higher ion-exchange capacity (126.4 meq $100g^{-1}$) than the synthetic K.SD phase (96.8 meq 100 g^{-1}), which would significantly impact the adsorption properties and capacities of the synthetic sodalite forms.

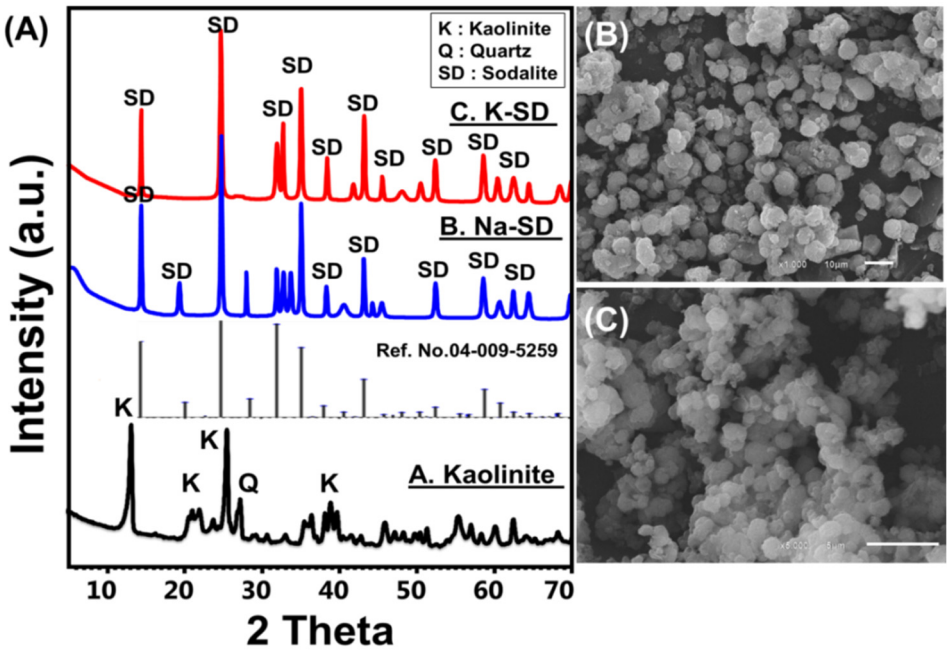

Figure 2. XRD patterns of kaolinite and the synthetic sodalite phases (**A**), SEM images of the prepared Na-sodalite (Na.SD) (**B**), and SEM images of K-sodalite (K.SD) (**C**).

Table 2. The textural properties of kaolinite, K.SD, and Na.SD.

Sample	Surface Area	Total Pore Volume	Average Pore Size	Cation-Exchange Capacity
Kaolinite	10 m^2 g^{-1}	0.072 cm^3 g^{-1}	43.2 nm	—-
K.SD	217.6 m^2 g^{-1}	0.214 cm^3 g^{-1}	9.7 nm	96.8 meq 100 g^{-1}
Na.SD	232.4 m^2 g^{-1}	0.247 cm^3 g^{-1}	7.4 nm	126.4 meq 100 g^{-1}

Such changes in the crystalline phase also appeared during the identification of the chemical functional groups based on the FT-IR spectra. The identified chemical groups of kaolinite as aluminosilicate structures were Si-O-Al (526 cm^{-1} and 680 cm^{-1}), Si-O (787 cm^{-1} as well as 456 cm^{-1}), Si-O-Si (1020 cm^{-1}), adsorbed O-H (1641 cm^{-1}), Al-OH (3500 cm^{-1} and 912 cm^{-1}), and Si-OH (3689 cm^{-1}) (Figure 3A) [38]. The synthetic zeolite phases exhibited similar chemical groups to kaolinite but at significant deviated positions, reflecting the impact of the alkaline conversion processes (Figure 3B,C). The recognized bands at 630–635 cm^{-1} for Na.SD and K.SD signify the symmetric stretching of Si-O-Si, which characterizes the zeolite structural units (Figure 3B,C) [39]. Additionally, the marked bands at 1475 cm^{-1} identify the water molecules within the structural channels and pores of the zeolite minerals, which confirm the conversion of kaolinite into zeolite [39].

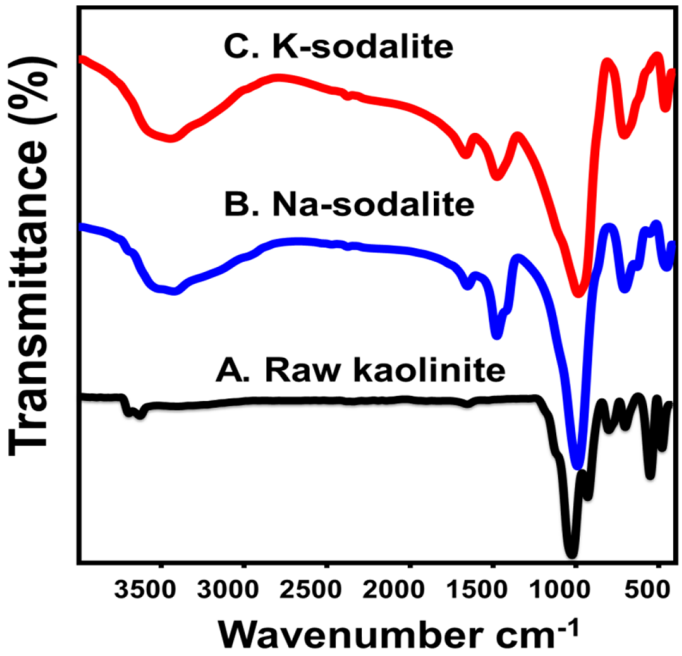

Figure 3. The FT–IR spectra of the used kaolinite (**A**), Na–sodalite (Na.SD) (**B**), and K–sodalite (K.SD) (**C**).

3.2. Adsorption Results

3.2.1. Effect of the Solution pH

The adjusted pH of the solutions during the sequestration of the dissolved anions, such as PO_4^{3-}, as well as the cation, significantly affected the present charges on the surface of the tested adsorbents as well as the ionization properties of the target adsorbate. Therefore, the sequestration of PO_4^{3-} by both K.SD and Na.SD was assessed within the experimental pH range from pH 3 to pH 8 considering the addressed concentration at 100 mg L^{-1}, the temperature at 20 °C, sodalite dosage at 0.1 g L^{-1}, and 240 min adsorption duration (Figure 4). The PO_4^{3-} sequestration efficiencies of both K.SD and Na.SD were highly pH-dependent as the determined capacities exhibited observable increments up to pH 6 (K.SD (72.7 mg g^{-1}) and Na.SD (86.3 mg g^{-1})) (Figure 4). These values clearly declined after conducting the tests at the higher pH conditions of pH 7 and pH 8, which can be attributed mainly to the ionization properties of the PO_4^{3-} ions (Figure 4). Dissolved phosphate ions exhibit neutral properties (H_3PO_4) at the acidic aqueous environments of pH less than 3 and acidic properties at the aqueous environments of pH higher than 3 up to the high-alkaline conditions (pH 3–7 ($H_2PO_4^-$) and pH higher than 7 (HPO_4^{2-} and PO_4^{3-})) as presented in Equations (5)–(7) [2,40]. Therefore, under highly acidic conditions, the neutral phosphate ions were of faint electrostatic attraction and ion-exchange properties with the effective groups of both K.SD and Na.SD. This enhanced gradually when increasing the pH to pH 6, where the conditions preserved the best quantities of the positive charges to attract the acidic phosphate ions ($H_2PO_4^-$) and enhance the ion replacement efficiency within the structures of the studied zeolite phases [24,41].

Increasing the pH toward alkaline environments caused adverse effects as the de-protonated surfaces of K.SD and Na.SD became saturated with negative charges which exhibited strong repulsive properties with the dominant acidic forms of phosphate at these conditions (HPO_4^{2-} and PO_4^{3-}). Therefore, pH 6 was selected to complete all the further studies of PO_4^{3-} adsorption in both K.SD and Na.SD. These results are also in agreement with determined pH_{ZPC} of K.SD (pH_{ZPC} = 8.2) and Na.SD (pH_{ZPC} = 8.7).

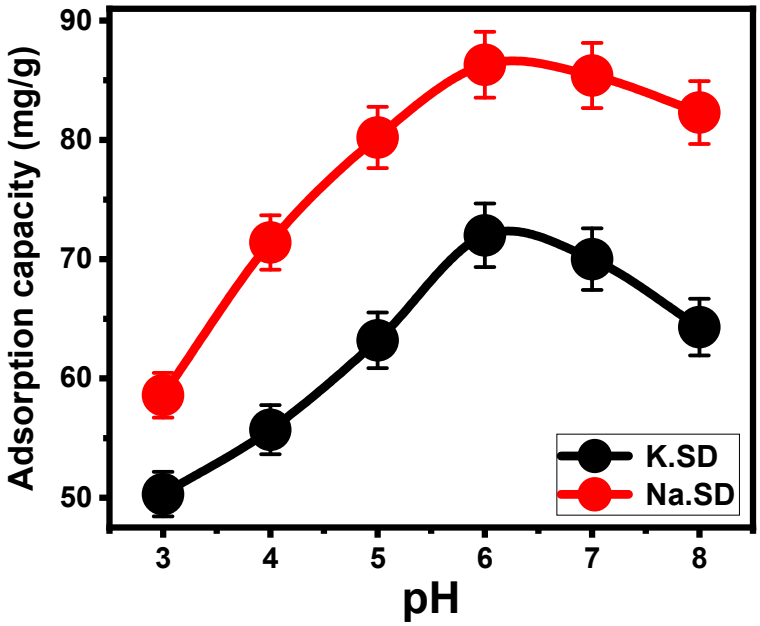

Figure 4. Effect of the solutions' pH on the sequestration of PO_4^{3-} of Na.SD and K.SD (100 mg L^{-1} phosphate concentration, 20 °C temperature, 0.1 g L^{-1} dosage, and 240 min adsorption duration).

$$H_3PO_4 \leftrightarrow H_2PO_4^- + H^+ \; pK_1 = 2.13 \quad (5)$$

$$H_2PO_4^- \leftrightarrow HPO_4^{2-} + H^+ \; pK_2 = 7.20 \quad (6)$$

$$HPO_4^{2-} \leftrightarrow PO_4^{3-} + H^+ \; pK_3 = 12.33 \quad (7)$$

3.2.2. Kinetic Studies

Effect of Contact Time

The sequestration behaviors of PO_4^{3-} ions by K.SD and Na.SD as a function of the adsorption duration was inspected from 30 min to 960 min considering the addressed concentration at 100 mg L^{-1}, the temperature at 20 °C, sodalite dosage at 0.1 g L^{-1}, and pH value at pH 6 (Figure 5A). The PO_4^{3-} sequestration capacity of both K.SD and Na.SD validates the remarkable enhancement with the uptake duration in addition to an observable change in the sequestration rates (Figure 5A). The K.SD and Na.SD adsorbents exhibited a strong sequestration rate from the start of the PO_4^{3-} uptake process to 240 min (Figure 5A). Following this, the actual sequestration rates declined strongly which was reflected in the faint changes in the determined phosphate sequestration capacity validating the equilibrium stages of K.SD and Na.SD as adsorbent systems of PO_4^{3-} with 85.2 mg g^{-1} and 100.3 mg g^{-1}, respectively, as equilibrium sequestration capacities (Figure 5A). The detectable change in the sequestration rates denotes the controlling effects of the availability of the free active sites during the reactions. The K.SD and Na.SD particles exhibited numerous free actives sites during the starting periods of the reaction, inducing the fast sequestration of the PO_4^{3-}. With the expansion of the test sequestration duration, the number of these sites declined regularly through occupying them with the PO_4^{3-} ions, causing declination in the sequestration rates. After the full occupation of these sites with the sequestrated PO_4^{3-}, the K.SD and Na.SD particles reached their equilibrium or saturation states and were unable to achieve more enhancements in their capacities [13].

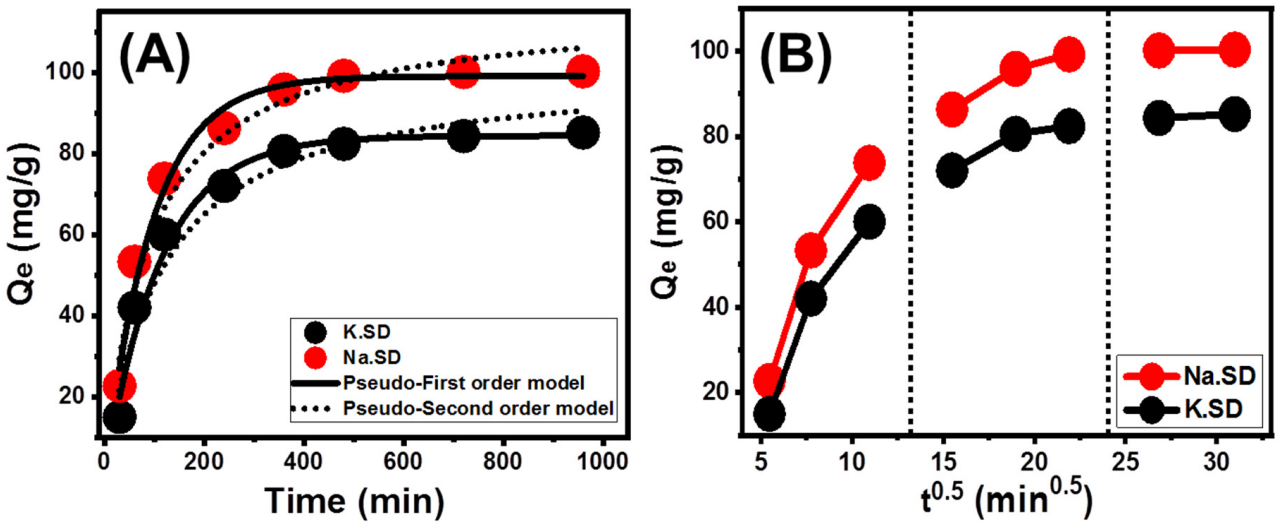

Figure 5. Effect of the duration time on the sequestration of PO_4^{3-} and its intraparticle diffusion properties (**A**), and fitting of the PO_4^{3-} sequestration results with the kinetic models (**B**) (100 mg L^{-1} phosphate concentration, 20 °C temperature, 0.1 g L^{-1} dosage, pH 6).

Kinetic Modeling

The sequestration kinetics of PO_4^{3-} by K.SD and Na.SD were described with the kinetic properties of both pseudo-first order (PFO) (Figure 5B) and pseudo-second order (PSO) (Figure 5B) as the investigated models. The determined values of the correlation coefficient (R^2) and chi-squared (χ^2) reflect the higher agreement between the PO_4^{3-} sequestration results and PFO than PSO (Figure 5B; Table 3). This suggested dominant effects for the physisorption reactions, especially the electrostatic attractive forces as compared to the chemical processes [42,43]. The significant matching between the experimentally detected Qe values (85.2 mg g^{-1} (K.SD) and 100.3 mg g^{-1} Na.SD) and the theoretically obtained values according to the pseudo-first-order model (86.4 mg g^{-1} (K.SD) and 102.09 mg g^{-1} Na.SD) induce the previous suggestion about the sequestration kinetic properties of PO_4^{3-} (Table 3). However, the remarkably high fitting results of the PO_4^{3-} sequestration reactions with the PSO model validate the operation of some assistant weak chemisorption processes (internal diffusion, electron sharing, electron exchange, and surface complexation) [2,42]. It was reported that the uptake of ions by both physical and chemical reactions can occur at the same time on the surfaces of the incorporated adsorbents involving the formation of a chemical adsorbed layer of the ions as substrates for several physically adsorbed layers [44].

Table 3. The mathematical parameters of the studied kinetic models.

Kinetic Models			
	Model	**Parameters**	**Values**
K.SD	Pseudo-first-order	K_1 (min^{-1})	0.0089
		$Qe_{(Cal)}$ (mg g^{-1})	84.4
		R^2	0.97
		X^2	0.52
	Pseudo-second-order	k_2 (mg g^{-1} min^{-1})	8.94×10^{-5}
		$Qe_{(Cal)}$ (mg g^{-1})	100.9
		R^2	0.95
		X^2	0.91

Table 3. *Cont.*

Kinetic Models			
	Model	**Parameters**	**Values**
Na.SD	Pseudo-first-order	K_1 (1 min^{-1})	0.010
		Qe $_{(Cal)}$ (mg g^{-1})	99.09
		R^2	0.98
		X^2	0.34
	Pseudo-second-order	k_2 (mg g^{-1} min^{-1})	9.77×10^{-5}
		Qe $_{(Cal)}$ (mg g^{-1})	115.79
		R^2	0.96
		X^2	0.66

Intraparticle Diffusion Behavior

The intraparticle-diffusion curves of K.SD and Na.SD as adsorption systems of PO_4^{3-} exhibited three detectable stages or steps of different slopes and showed no intersections with the points of origin (Figure 5A). These properties validate the sequestration of phosphate by more than one mechanism involving the diffusion process of the PO_4^{3-} ions toward K.SD and Na.SD adsorbents [45,46]. The following mechanisms may be included: (A) external surface (border) reactions, (B) intraparticle diffusion processes, and (C) the saturation and/or equilibrium and their effects [47]. The starting or firstly operated sequestration mechanism based on the first segments of the curves is related to the external uptake processes via the surficial active functional groups and regulated mostly by the availability and exposure of these groups (Figure 5A) [34]. Detecting the second stage as intermediate sections in the curves reflected that the effect of the external processes completely faded away and the dominance of other processes related to the layered uptake mechanisms and the intraparticle diffusion effects (Figure 5A) [46,47]. During this stage, the PO_4^{3-} ions diffused strongly within the internal channels and structure of K.SD and N.SD zeolite, and interacted effectively with the present active chemical groups [47,48]. By observing the equilibration stages, the third segment can be detected which denotes the full occupation and consumption of all the binding sites of the K.SD and Na.SD particles (Figure 5A). This segment signifies the impact of the molecular interaction and interionic attraction processes as the controlling mechanisms during the sequestration of phosphate ions [27,49].

3.2.3. Equilibrium Studies

Effect of PO_4^{3-} Concentration

The sequestration properties of both K.SD and Na.SD in terms of the evaluated concentrations of PO_4^{3-} (50 mg L^{-1} up to 350 mg L^{-1}) demonstrate their experimental maximum capacities, as well as their equilibrium behaviors (Figure 6A). The essential experimental conditions were adjusted at 960 min for the adsorption duration, 20 °C for the sequestration temperature, 0.1 g L^{-1} for the sodalite dosage, and pH 6. The sequestration capacities of K.SD and Na.SD were enhanced significantly in terms of the starting PO_4^{3-} concentrations in the aqueous solutions from 50 mg/L to 200 mg/L (Figure 6A). The previous literature reported a significant impact of the high initial concentrations on the driving forces and in turn the diffusion and mobility properties of the ions. Therefore, the collision and interaction chances between the diffused PO_4^{3-} and the surfaces of K.SD as well as Na.SD strongly enhance with these concentrations [50]. The tests that were conducted with PO_4^{3-} concentrations higher than 200 mg/L resulted in neglected or nearly fixed sequestration capacities which signified this value as being the equilibrium concentration at which the K.SD and Na.SD particles achieved their saturation or maximum sequestration capacities (126 mg g^{-1} (K.SD) and 165 mg g^{-1} Na.SD) (Figure 6A). These curves exhibit the L-type isotherm properties according to Giles's classification which suggests complete sequestration of the PO_4^{3-} ions in monolayer forms and the existence of intermolecular attractive forces (Figure 6A) [51–53].

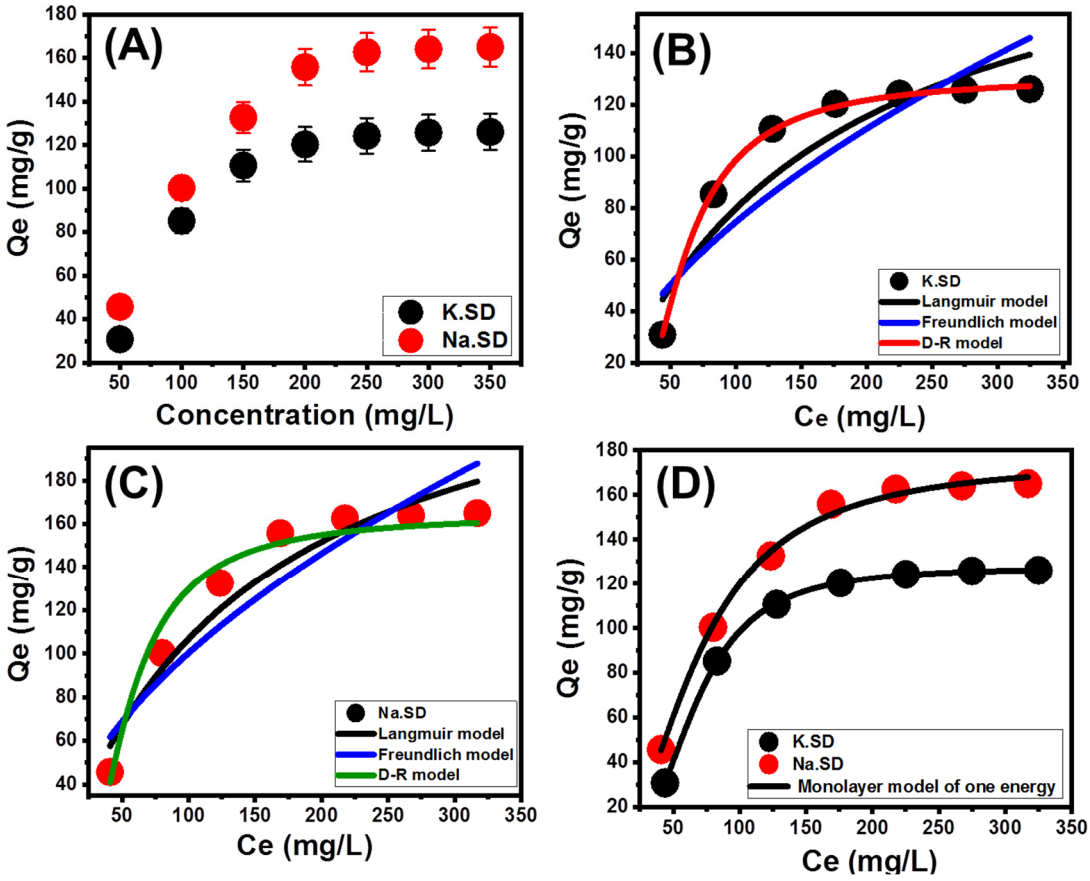

Figure 6. Effect of the PO_4^{3-} concentrations on the sequestration capacities of Na.SD and K.SD (**A**), fitting of the PO_4^{3-} sequestration results of K.SD with different isotherm models (**B**), fitting of the sequestration results of Na.SD with different isotherm models (**C**), and fitting of the sequestration results with the advanced monolayer model of one energy site (**D**) (pH 6, 20 °C temperature, 0.1 g L^{-1} dosage, and 960 min adsorption duration).

Classic Isotherm Models

The assessed classic models illustrate the equilibrium behaviors of the PO_4^{3-} sequestration reactions of both K.SD (Figure 6B) and Na.SD (Figure 6C), these involved Langmuir and Freundlich models in addition to the D-R equilibrium model. Considering the determined R^2 (determination coefficient) and χ^2 (chi-squared) for the performed nonlinear fitting processes, the sequestration of PO_4^{3-} by K.SD and Na.SD adsorption systems follow the equilibrium properties of Langmuir isotherm (Table 4). The Langmuir isotherm properties validate the sequestration of PO_4^{3-} in Monolayer forms with a controlling effect for the present active sites which distribute homogeneously on the surfaces of K.SD and Na.SD [34,49]. The theoretically obtained PO_4^{3-} Q_{max} values of K.SD and Na.SD, as fitting parameters, were 201.9 mg g^{-1} and 261.6 mg g^{-1}, respectively (Table 4).

The other assessed classic isotherm model was the D-R model which exhibits valuable significance in the apparent energetic heterogeneity properties of homogenous as well as heterogeneous uptake systems [54]. Moreover, the parameters of this model validate the type of operated mechanisms (physisorption or chemisorption) during the sequestration of PO_4^{3-} by K.SD and Na.SD based on the theoretically determined values of Gaussian energy (E) (<8 KJ mol^{-1} (physisorption), 8 KJ mol^{-1} to 16 KJ mol^{-1} (weak chemisorption and ion-exchange processes), and >16 KJ mol^{-1} (strong chemisorption processes and formation of bonds)) [49,54]. Therefore, the obtained E values for the sequestration of PO_4^{3-} by K.SD and Na.SD were 6.5 KJ mol^{-1} and 7.1 KJ mol^{-1}, respectively (Table 4). These values are within validating physisorption to weak chemisorption sequestration reactions. Moreover,

these values are within the signified range of zeolite ion-exchange reactions (0.6 KJ mol^{-1} to 25 KJ mol^{-1}) [13].

Table 4. Mathematical parameters of the evaluated classic and advanced isotherm models.

Isotherm Models			
Classic Isotherm Models			
K.SD	Langmuir model	Q_{max} (mg g^{-1})	201.9
		b(L mg^{-1})	0.0061
		R^2	0.90
		X^2	2.9
	Freundlich model	$1/n$	0.570
		k_F (mg g^{-1})	5.37
		R^2	0.84
		X^2	4.74
	D-R model	β (mol^2 KJ^{-2})	0.0117
		Q_m (mg g^{-1})	130.6
		R^2	0.99
		X^2	0.011
		E (KJ mol^{-1})	6.5
Na.SD	Langmuir model	Q_{max} (mg g^{-1})	261.6
		b(L mg^{-1})	0.0069
		R^2	0.95
		X^2	1.56
	Freundlich model	$1/n$	0.544
		k_F (mg g^{-1})	8.19
		R^2	0.87
		X^2	3.44
	D-R model	β (mol^2 KJ^{-2})	0.01977
		Q_m (mg g^{-1})	164.3
		R^2	0.98
		X^2	0.69
		E (KJ mol^{-1})	7.15
Advanced Isotherm model			
Steric and Energetic Parameters			
K.SD		R^2	0.996
		X^2	0.0019
		n	2.86
		N_m (mg $g^{-1)}$	44.4
		Q_{Sat} (mg g^{-1})	127.4
		C1/2 (mg L^{-1})	65.24
		ΔE (kJ mol^{-1})	17.72
Na.SD		R^2	0.997
		X^2	0.06
		n	2.03
		N_m (mg $g^{-1)}$	86.1
		Q_{Sat} (mg g^{-1})	175.39
		C1/2 (mg L^{-1})	68.57
		ΔE (kJ mol^{-1})	18.04

Advanced Equilibrium Studies

The suggested equilibrium models based on the assumptions of the statistical physics theory are valuable for the illustration of the sequestration mechanisms when considering the adsorbate/adsorbent interactions in terms of the active site's density (Nm), the number of sequestrated PO_4^{3-} in each site (n), saturation sequestration capacity (Q_{sat}),

and sequestration energy (ΔE) (Table 3). The mathematical parameters of the representative advanced monolayer model of one energy site (Figure 6D) demonstrate the enrichments of the Na.SD particles with higher quantities of active sequestration sites (Nm = 86.1 mg g^{-1}) as compared to the K.SD particles (Nm = 44.4 mg g^{-1}) which might be related to the high reactivity of their sodium content and their higher ion-exchange properties (Table 4). This also illustrates the remarkable higher PO_4^{3-} sequestration capacities of Na.SD (Q_{sat} = 175.39 mg g^{-1}) compared to K.SD (Q_{sat} = 127.4 mg g^{-1}) at the saturation states of their incorporated particles (Table 4). The present sequestration sites on the surfaces of both K.SD (*n* = 2.86) and Na.SD (*n* = 2.03) exhibit capacities to adsorb 2 to 3 PO_4^{3-} ions at each site (Table 4). This reflects the sequestration of the dissolved PO_4^{3-} ions by multi-ionic mechanisms and the orientation of these ions in vertical and nonparallel forms [55,56]. The sequestration energies (ΔE) of PO_4^{3-} in K.SD and Na.SD were calculated according to Equation (8), considering the concentration of the phosphate ions at the half-saturation states of the two sodalite forms.

$$\Delta E = -RT \ln\left(\frac{S}{C1/2}\right) \quad (8)$$

The determined ΔE values for the sequestration reactions of K.SD and Na.SD were 18.2 KJ mol^{-1} and 18.04 KJ mol^{-1}, respectively (Table 3). These values are within the reported ranges for physisorption processes or weak chemisorption reactions (<40 KJ mol^{-1}) which may involve dipole bonding forces (2–29 kJ/mol), van der Waals forces (4–10 KJ mol^{-1}), and hydrogen bonding (<30 KJ mol^{-1}) [55].

3.2.4. Effect of Dosages

The sequestration efficiency of PO_4^{3-} in terms of the applied K.SD and Na.SD dosages were evaluated from 0.1 g L^{-1} to 0.5 g L^{-1}. The essential experimental conditions were adjusted at 960 min for the adsorption duration, 20 °C for the sequestration temperature, 50 mg L^{-1} for the PO_4^{3-} concentration, and pH 6. The incorporation of K.SD at 0.1 g L^{-1}, 0.2 g L^{-1}, 0.3 g L^{-1}, 0.4 g L^{-1}, and 0.5 g L^{-1} as dosages induced the sequestration percentages of PO_4^{3-} by 12.3%, 27.4%, 44.6%, 62.7%, and 77.8%, respectively (Figure 7). For the incorporated dosages of Na.SD, the sequestration percentages increased by 18.3% (0.1 g L^{-1}), 38.6% (0.2 g L^{-1}), 63% (0.3 g L^{-1}), 80.2% (0.4 g L^{-1}), and 98.4% (0.5 g L^{-1}) (Figure 7). The significant high sequestration efficiencies of PO_4^{3-} in the presence of both K.SD and Na.SD at high dosages was attributed in the literature to the associated increase in the interact surface area and quantities of free active sites [57]. Moreover, these results demonstrate the high efficiency of the two sodalite products to be applied in the sequestration of phosphate from both industrial wastewater and agricultural drainage water.

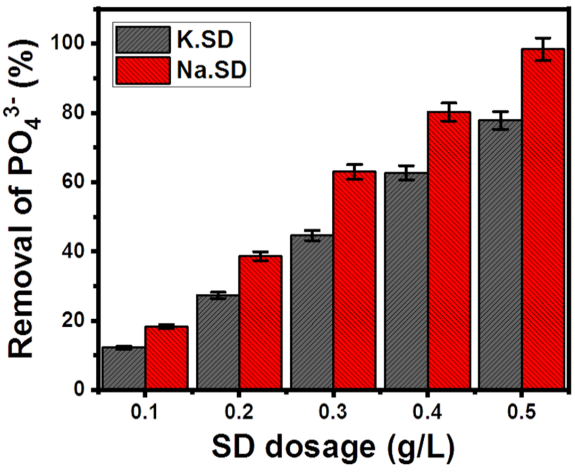

Figure 7. Effect of the K.SD and Na.SD dosages on the sequestration percentages of PO_4^{3-} (pH 6, 20 °C temperature, 50 mg L^{-1} phosphate concentration, and 960 min adsorption duration).

3.2.5. Thermodynamic Properties

The thermodynamic properties of K.SD and Na.SD as sequestration systems of PO_4^{3-} were described in terms of Gibbs free energy (ΔG°) in addition to the values of enthalpy (ΔH°) and entropy (ΔS°). The essential experimental conditions were adjusted at 960 min for the adsorption duration, 0.1 g/L for the adsorption dosage, 100 mg L^{-1} for the PO_4^{3-} concentration, and pH 6, with a temperature range of 20 °C to 50 °C. The theoretically estimated ΔG° was obtained from Equation (9) while the values of ΔH° and ΔS° were determined to be fitting parameters of the Van't Hoff equation (Equation (10)) (Figure 8) [17].

$$\Delta G^0 = -RT \ln K_c \quad (9)$$

$$\ln (K_c) = \frac{\Delta S^o}{R} - \frac{\Delta H^o}{RT} \quad (10)$$

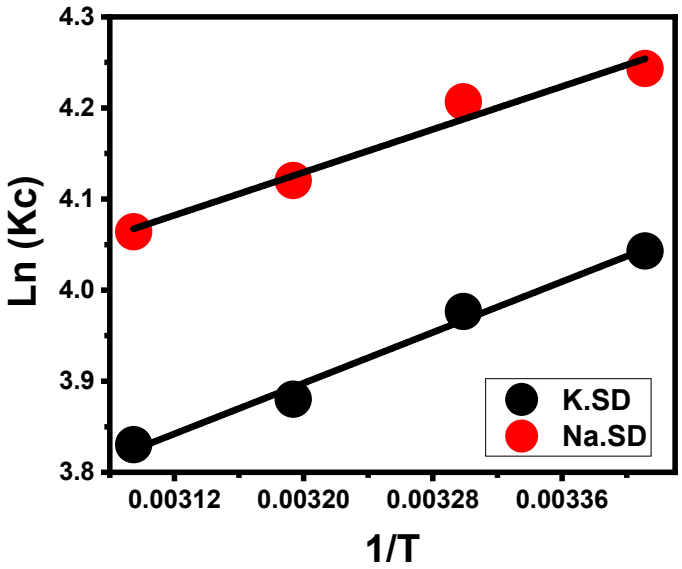

Figure 8. Fitting of the PO_4^{3-} sequestration results with Van't Hoff equation (pH 6, 100 mg L^{-1} phosphate concentration, 0.1 g L^{-1} dosage, and 960 min adsorption duration).

The determined values of ΔG° and ΔH° exhibit negative signs which validate the spontaneous and exothermic sequestration of PO_4^{3-} by both K.SD and Na.SD (Table 4). Moreover, the determination of ΔS° at positive signs during the sequestration processes using K.SD and Na.SD demonstrates the increment in the randomness properties of the adsorption systems at high-temperature conditions (Table 5) [57].

Table 5. The thermodynamic parameters of the phosphate sequestration reactions of K.SD and Na.SD.

Thermodynamic Parameters			
Parameters	**Temperature**	**K.SD**	**Na.SD**
ΔG° (kJ mol^{-1})	293.13	−9.85	−10.34
	303.13	−10.02	−10.60
	313.13	−10.10	−10.72
	323.13	−10.29	−10.91
ΔH° (kJ mol^{-1})		−5.78	−4.89
ΔS° (J $K^{-1}mol^{-1}$)		14.63	18.67

3.2.6. Recyclability

The recyclability and suitability of the K.SD and Na.SD particles to be used several times signify the values of the products to be applied effectively in the realistic and com-

mercial sequestration of PO_4^{3-}. The regeneration of the sodalite fractions involved careful washing of the K.SD and Na.SD particles with distilled water for four runs with the duration of each washing run being 15 min. After that, the washed K.SD and Na.SD were dried for 12 h at 60 °C using an electric digital drier and then the dried products were reused again in another sequestration run. The essential experimental conditions were adjusted at 960 min for the adsorption duration, 0.5 g L^{-1} for the sodalite dosage, 20 °C for the adsorption temperature, 50 mg L^{-1} for the PO_4^{3-} concentration, and pH 6. The determined PO_4^{3-} sequestration percentages of both K.SD and Na.SD demonstrates their high stability and recyclability (Figure 9). The recognized PO_4^{3-} sequestration percentages of K.SD during the assessed runs were 77.8% (Run 1), 77% (Run 2), 72.3% (Run 3), 66.2% (Run 4), and 57.4% (Run 5) (Figure 9). During the recyclability tests of Na.SD, the determined sequestration percentages were 98.4% (Run 1), 95.2% (Run 2), 90.7% (Run 3), 84.3% (Run 4), and 75.8 % (Run 5) (Figure 9). Such results are highly promising considering the tested phosphate concentrations (50 mg L^{-1}).

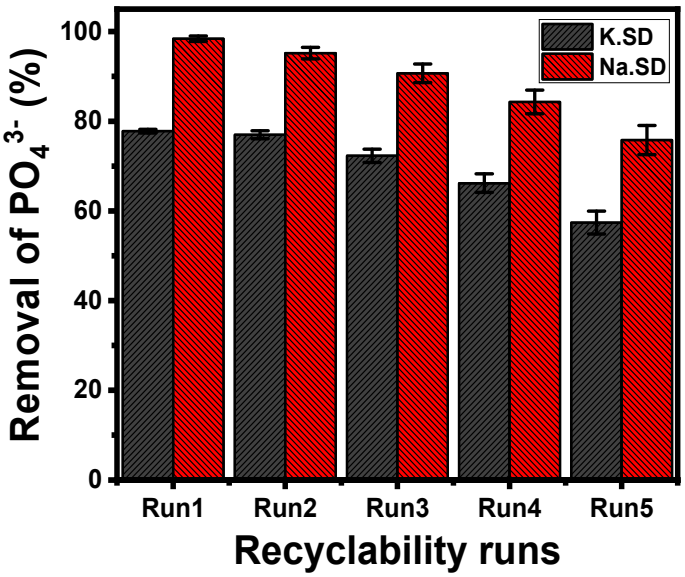

Figure 9. The recyclability properties of synthetic K.SD and Na.SD during the sequestration of PO_4^{3-} equation (pH 6, 50 mg L^{-1} phosphate concentration, 0.1 g L^{-1} dosage, and 960 min adsorption duration).

3.2.7. Effect of Coexisting Anions

The expected negative impacts of the other dissolved competitive or coexisting anions during the sequestration of PO_4^{3-} by both K.SD and Na.SD were followed in the existence of Cl^-, SO_4^{2-}, HCO_3^-, and NO_3^- anions. The essential experimental conditions were adjusted at 960 min for the adsorption duration, 0.5 g L^{-1} for the sodalite dosage, 20 °C for the adsorption temperature, 50 mg L^{-1} concentration (50% PO_4^{3-}: 50% another anion), and pH 6. The determined sequestration percentages of both K.SD and Na.SD reflect the considerable competitive and negative impacts of HCO_3^- during the sequestration of PO_4^{3-} from the aqueous solutions (Figure 10). The other investigated anions (Cl^-, SO_4^{2-}, and NO_3^-) exhibit slight or neglected competitive effects during the sequestration of PO_4^{3-} by K.SD as well as Na.SD (Figure 10). This behavior can be determined based on the ligand exchange and complexation processes that control the sequestration reactions [13,40]. The sequestrated PO_4^{3-} and HCO_3^- of sodalite structures tend to form inner-sphere complexes which exhibit high stability as compared to the adsorbed Cl^-, SO_4^{2-}, and NO_3^- anions which give the HCO_3^- ions higher competitive effects than them [40].

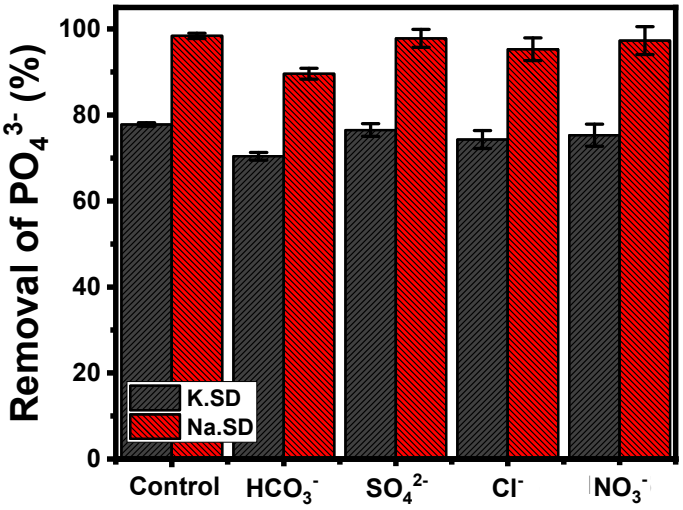

Figure 10. Effect of the coexisting anions on the affinities of K.SD and Na.SD for PO_4^{3-} (pH 6, 50 mg L^{-1} phosphate concentration, 0.1 g L^{-1} dosage, and 960 min adsorption duration).

3.2.8. Comparison Study

The achieved PO_4^{3-} sequestration capacities of both K.SD and Na.SD in two phases of sodalite were compared with other investigated adsorbents in the literature (Table 6). The two sodalite phases which were formed by low-temperature alkali fusion of kaolinite exhibited higher capacities than several synthetic structures such as Zirconia/graphite oxide, La doping magnetic graphene, calcined Mg-Al-LDHs, $Mg(OH)_2/ZrO_2$, Mg/Al modified biochar, ZrO_2 nanoparticles, and Lanthanum hydroxides. This demonstrates the value of both K.SD and Na.SD, as they are environmentally friendly, recyclable, low-cost, and very effective adsorbents of PO_4^{3-}, which can be reused as an eco-friendly fertilizer.

Table 6. The estimated PO_4^{3-} sequestration capacities of K.SD and Na.SD as compared to other studied materials.

Adsorbents	Q_{max} (mg g^{-1})	References
MCM-41/Rice husk	21	[58]
Lanthanum hydroxides	107.5	[59]
Fe−Mn binary oxide	36	[60]
$Mg(OH)_2/ZrO_2$	87.2	[47]
Biochar	133	[61]
La doping magnetic graphene	116.28	[62]
Mg/Al modified biochar	56.12	[5]
Calcined Mg-Al-LDHs	40.78	[63]
Zirconia/graphite oxide	149.3	[64]
Titanium modified zeolite	37.60	[65]
Titania/GO	33.11	[66]
ZrO_2 nanoparticles	99	[67]
Kaolintic clay	38.46	[68]
Hydrous zirconium oxide	51.8	[69]
K.SD	127.4	This study
Na.SD	175.39	This study

3.2.9. Realistic Study

The synthetic products were applied in the realistic adsorption of the PO_4^{3-} ions in the Rákos-stream real-water sample (500 mL) with an initial concentration of 0.52 mg L^{-1}, 0.5 g L^{-1} of both K.SD and Na.SD mixed with the water samples at pH 6, and a temperature of 20 °C. The sequestration percentages were assessed within experimental intervals from 20 min to 120 min. The obtained results reflected the complete adsorption of the present PO_4^{3-} ions in Rákos-stream real-water after 20 min using Na.SD and after 60 min using

K.SD. This signifies the significant efficiencies of both K.SD and Na.SD when used in the realistic remediation and adsorption processes of PO_4^{3-} ions from the Rákos stream and within the recommended European standards (0.2 mg L^{-1}). The slower sequestration rates of PO_4^{3-} from the Rákos-stream real-water in K.SD and Na.SD and their lower capacities than the presented results from the aqueous solutions validate the significant effects of the other dissolved cations and anions in the water from the stream as a natural water resource.

3.2.10. Suggested Mechanism

The adsorption mechanism of phosphate by the synthetic sodalite phases was suggested based on the previous literature and the estimated theoretical properties based on classic and advanced equilibrium studies. The removal of phosphate occurs mainly by ion-exchange reactions with exchange ions within the zeolite pores and within its structures, as presented in Equation (11) [4,13]. Moreover, other essential mechanisms were reported as effective mechanisms during the uptake of phosphate by zeolite-based adsorbents including electrostatic attractions and the formation of chemical complexes or weak chemical bonds [4,70]. Phosphate ions tend to create types of monodentate and bidentate chemical complexes with the active binding sites of the silicate structure of zeolite (Figure 9) [13].

$$SD - K^+,\ Na^+ + H_2PO_4^- \rightarrow K^+,\ Na^+ + SD - H_2PO_4^- \quad (11)$$

4. Conclusions

Two sodalite phases were synthesized using two different alkaline solutions (KOH and NaOH) as synthetic zeolite of different alkali-bearing structures (K-rich phase (K.SD) and Na-rich sodalite (Na.SD)) through the alkali fusion processes of kaolinite as enhanced adsorbents of phosphate ions from water. The two phases were applied effectively in the decontamination of PO_4^{3-} in an aqueous environment and the water of the Rákos stream in comparative studies. The Na.SD phase exhibited higher sequestration capacity (Qsat = 175.3 mg g^{-1}) than the K.SD phase (Qsat = 127.4 mg g^{-1}). This was attributed to the enhanced surface area (232.4 m^2 g^{-1}), ion-exchange capacity (126.4 meq 100 g^{-1}), and the active site density (Nm = 86.1 mg g^{-1}) of Na.SD as compared to K.SD. The sequestrations of PO_4^{3-} either by Na.SD or K.SD are exothermic, homogenous, and spontaneous processes considering their thermodynamic and equilibrium functions. The estimated values of Gaussian energy as well as the adsorption energy suggest the sequestration of PO_4^{3-} by physisorption and weak chemisorption mechanisms including zeolitic ion-exchange reactions. The synthetic phases are of significant affinity for the dissolved phosphate ions even in the coexistence of Cl^-, SO_4^{2-}, HCO_3^-, and NO_3^- as competitive anions. The realistic application of these results in the complete adsorption of PO_4^{3-} from Rákos-stream water after 20 min (Na.SD) and 60 min (K.SD).

Supplementary Materials: The following supporting information can be downloaded at: https://www.mdpi.com/article/10.3390/inorganics11010014/s1, Figure S1: SEM image of the used kaolinite precursor during the synthesis of the sodalite phases; Table S1: analysis of the studied raw water sample.

Author Contributions: Conceptualization, S.B., M.R.A., I.F., S.P., A.A.A. and M.H.E.; methodology, M.H.E., S.P., M.R.A.; software, M.H.E., S.P.; validation, S.B., M.R.A., I.F., S.P., A.K., J.S.A., S.I.O.; formal analysis, M.H.E., S.P., A.A.A.; investigation, J.S.A., S.I.O., A.A.A., M.R.A.; resources, S.B., M.R.A., M.H.E., J.S.A., S.I.O.; data curation, M.H.E., A.K., M.R.A.; writing—original draft preparation, M.R.A., I.F., M.H.E., J.S.A., S.I.O.; writing—review and editing, S.B., M.R.A., A.K., M.H.E., A.A.A., S.P.; visualization, M.R.A., J.S.A., A.A.A., S.I.O.; supervision, S.B., A.A.A., M.R.A., I.F., A.K., I.F.; project administration, J.S.A., S.I.O.; funding acquisition, J.S.A., S.I.O.; All authors have read and agreed to the published version of the manuscript.

Funding: This research was funded by [King Saud University] Project number [RSP2023R149] and [Princess Nourah bint Abdulrahman University] Project number [PNURSP2022R5].

Data Availability Statement: Data are available upon reasonable, by the Corresponding Authors.

Acknowledgments: The authors acknowledge Researchers Supporting Project number (RSP2023R149), King Saud University, Riyadh, Saudi Arabia. Also, the authors acknowledge Princess Nourah bint Abdulrahman University Researchers Supporting Project number (PNURSP2022R5), Princess Nourah bint Abdulrahman University, Riyadh, Saudi Arabia.

Conflicts of Interest: The authors declare no conflict of interest.

References

1. Fang, L.; Zeng, W.; Xu, L.; Huang, L.-Z. Green rusts as a new solution to sequester and stabilize phosphate in sediments under anoxic conditions and their implication for eutrophication control. *Chem. Eng. J.* **2020**, *388*, 124198. [CrossRef]
2. Salam, M.A.; Mokhtar, M.; Albukhari, S.M.; Baamer, D.F.; Palmisano, L.; AlHammadi, A.A.; Abukhadra, M.R. Synthesis of zeolite/geopolymer composite for enhanced sequestration of phosphate (PO_4^{3-}) and ammonium (NH_4^+) ions; equilibrium properties and realistic study. *J. Environ. Manag.* **2021**, *300*, 113723. [CrossRef] [PubMed]
3. Peng, X.; Wang, M.; Hu, F.; Qiu, F.; Dai, H.; Cao, Z. Facile fabrication of hollow biochar carbon-doped TiO_2/CuO composites for the photocatalytic degradation of ammonia nitrogen from aqueous solution. *J. Alloy. Compd.* **2018**, *770*, 1055–1063. [CrossRef]
4. Mokrzycki, J.; Fedyna, M.; Marzec, M.; Szerement, J.; Panek, R.; Klimek, A.; Bajda, T.; Mierzwa-Hersztek, M. Copper ion-exchanged zeolite X from fly ash as an efficient adsorbent of phosphate ions from aqueous solutions. *J. Environ. Chem. Eng.* **2022**, *10*, 108567. [CrossRef]
5. Deng, Y.; Li, M.; Zhang, Z.; Liu, Q.; Jiang, K.; Tian, J.; Zhang, Y.; Ni, F. Comparative study on characteristics and mechanism of phosphate adsorption on Mg/Al modified biochar. *J. Environ. Chem. Eng.* **2021**, *9*, 105079. [CrossRef]
6. Munar-Florez, D.A.; Varón-Cardenas, D.A.; Ramírez-Contreras, N.E.; García-Núñez, J.A. Adsorption of ammonium and phosphates by biochar produced from oil palm shells: Effects of production conditions. *Results Chem.* **2021**, *3*, 100119. [CrossRef]
7. Boromisza, Z.; Illyés, Z.; Gergely, A.; Mészáros, S.; Monspart-Molnár, Z. Evaluation of the possibilities for stream restoration: Preassessment of the Váli-stream (Hungary). *Landsc. Environ.* **2016**, *10*, 26–44. [CrossRef]
8. Asaoka, S.; Kawakami, K.; Saito, H.; Ichinari, T.; Nohara, H.; Oikawa, T. Adsorption of phosphate onto lanthanum-doped coal fly ash—Blast furnace cement composite. *J. Hazard. Mater.* **2020**, *406*, 124780. [CrossRef]
9. Buyanjargal, A.; Kang, J.; Sleep, B.E.; Jeen, S.-W. Sequential treatment of nitrate and phosphate in groundwater using a permeable reactive barrier system. *J. Environ. Manag.* **2021**, *300*, 113699. [CrossRef]
10. Arshadi, M.; Abdolmaleki, M.; Eskandarloo, H.; Azizi, M.; Abbaspourrad, A. Synthesis of Highly Monodispersed, Stable, and Spherical NZVI of 20–30 nm on Filter Paper for the Removal of Phosphate from Wastewater: Batch and Column Study. *ACS Sustain. Chem. Eng.* **2018**, *6*, 11662–11676. [CrossRef]
11. Van Truong, T.; Kim, D.-J. Phosphate removal using thermally regenerated Al adsorbent from drinking water treatment sludge. *Environ. Res.* **2021**, *196*, 110877. [CrossRef] [PubMed]
12. Abali, M.; Ichou, A.A.; Zaghloul, A.; Sinan, F.; Zerbet, M. Removal of nitrate ions by adsorption onto micro-particles of shrimp-shells waste: Application to wastewater of infiltration-percolation process of the city of Agadir (Morocco). *Mater. Today: Proc.* **2020**, *37*, 3898–3904. [CrossRef]
13. El-Sherbeeny, A.M.; Soliman, S.R.; AlHammadi, A.A.; Shim, J.-J.; Abukhadra, M.R. Insight into the CaO green decorated clinoptilolite as an effective adsorbent for nitrate and phosphate ions; equilibrium; kinetic, and safety studies. *Surfaces Interfaces* **2021**, *27*, 101568. [CrossRef]
14. Karthikeyan, P.; Meenakshi, S. Development of sodium alginate@ZnFe-LDHs functionalized beads: Adsorption properties and mechanistic behaviour of phosphate and nitrate ions from the aqueous environment. *Environ. Chem. Ecotoxicol.* **2020**, *3*, 42–50. [CrossRef]
15. Lei, H.; Muhammad, Y.; Wang, K.; Yi, M.; He, C.; Wei, Y.; Fujita, T. Facile fabrication of metakaolin/slag-based zeolite microspheres (M/SZMs) geopolymer for the efficient remediation of Cs^+ and Sr^{2+} from aqueous media. *J. Hazard. Mater.* **2021**, *406*, 124292. [CrossRef]
16. Wang, Y.; Song, X.; Xu, Z.; Cao, X.; Song, J.; Huang, W.; Ge, X.; Wang, H. Adsorption of Nitrate and Ammonium from Water Simultaneously Using Composite Adsorbents Constructed with Functionalized Biochar and Modified Zeolite. *Water Air Soil Pollut.* **2021**, *232*, 1–19. [CrossRef]
17. Jiao, Z.; Meng, Y.; He, C.; Yin, X.; Wang, X.; Wei, Y. One-pot synthesis of silicon-based zirconium phosphate for the enhanced adsorption of Sr (II) from the contaminated wastewater. *Microporous Mesoporous Mater.* **2021**, *318*, 111016. [CrossRef]
18. Jiang, Y.; Abukhadra, M.R.; Refay, N.M.; Sharaf, M.F.; El-Meligy, M.A.; Awwad, E.M. Synthesis of chitosan/MCM-48 and β-cyclodextrin/MCM-48 composites as bio-adsorbents for environmental removal of Cd2+ ions; kinetic and equilibrium studies. *React. Funct. Polym.* **2020**, *154*, 104675. [CrossRef]
19. Li, B.; Xue, Q.; Wan, Y.; Liu, L.; Fu, J.; Yu, Y.; Wang, F.; Li, J.; Zhang, F.; Zhang, S.; et al. Substantial and rapid phosphorous adsorption by calcium modified mesoporous silicon micropheres. *Chem. Eng. J. Adv.* **2021**, *7*, 100124. [CrossRef]
20. Kumar, I.A.; Jeyaseelan, A.; Viswanathan, N.; Naushad, M.; Valente, A.J. Fabrication of lanthanum linked trimesic acid as porous metal organic frameworks for effective nitrate and phosphate adsorption. *J. Solid State Chem.* **2021**, *302*, 122446. [CrossRef]

21. Yin, Q.; Ren, H.; Wang, R.; Zhao, Z. Evaluation of nitrate and phosphate adsorption on Al-modified biochar: Influence of Al content. *Sci. Total. Environ.* **2018**, *631–632*, 895–903. [CrossRef] [PubMed]
22. Wang, Y.; Zhao, W.; Qi, Z.; Zhang, L.; Zhang, Y.; Huang, H.; Peng, Y. Designing ZIF-8/hydroxylated MWCNT nanocomposites for phosphate adsorption from water: Capability and mechanism. *Chem. Eng. J.* **2020**, *394*, 124992. [CrossRef]
23. Park, J.Y.; Lee, J.; Go, G.-M.; Jang, B.; Cho, H.-B.; Choa, Y.-H. Removal performance and mechanism of anti-eutrophication anions of phosphate by CaFe layered double hydroxides. *Appl. Surf. Sci.* **2021**, *548*, 149157. [CrossRef]
24. Abukhadra, M.R.; Mostafa, M. Effective decontamination of phosphate and ammonium utilizing novel muscovite/phillipsite composite; equilibrium investigation and realistic application. *Sci. Total Environ.* **2019**, *667*, 101–111. [CrossRef]
25. Alshameri, A.; He, H.; Zhu, J.; Xi, Y.; Zhu, R.; Ma, L.; Tao, Q. Adsorption of ammonium by different natural clay minerals: Characterization, kinetics and adsorption isotherms. *Appl. Clay Sci.* **2017**, *159*, 83–93. [CrossRef]
26. Nasief, F.; Shaban, M.; Alamry, K.A.; Abu Khadra, M.R.; Khan, A.A.P.; Asiri, A.M.; El-Salam, H.A. Hydrothermal synthesis and mechanically activated zeolite material for utilizing the removal of Ca/Mg from aqueous and raw groundwater. *J. Environ. Chem. Eng.* **2021**, *9*, 105834. [CrossRef]
27. Salam, M.A.; Abukhadra, M.R.; Mostafa, M. Effective decontamination of As(V), Hg(II), and U(VI) toxic ions from water using novel muscovite/zeolite aluminosilicate composite: Adsorption behavior and mechanism. *Environ. Sci. Pollut. Res.* **2020**, *27*, 13247–13260. [CrossRef]
28. Simanjuntak, W.; Pandiangan, K.D.; Sembiring, Z.; Simanjuntak, A.; Hadi, S. The effect of crystallization time on structure, microstructure, and catalytic activity of zeolite-A synthesized from rice husk silica and food-grade aluminum foil. *Biomass-Bioenergy* **2021**, *148*, 106050. [CrossRef]
29. Rios, C.A.; Williams, C.; Fullen, M.A. Nucleation and growth history of zeolite LTA synthesized from kaolinite by two different methods. *Appl. Clay Sci.* **2009**, *42*, 446–454. [CrossRef]
30. Mokrzycki, J.; Fedyna, M.; Marzec, M.; Panek, R.; Szerement, J.; Marcińska-Mazur, L.; Jarosz, R.; Bajda, T.; Franus, W.; Mierzwa-Hersztek, M. The influence of zeolite X ion-exchangeable forms and impregnation with copper nitrate on the adsorption of phosphate ions from aqueous solutions. *J. Water Process. Eng.* **2022**, *50*, 103299. [CrossRef]
31. Capa-Cobos, L.F.; Jaramillo-Fierro, X.; González, S. Computational Study of the Adsorption of Phosphates as Wastewater Pollutant Molecules on Faujasites. *Processes* **2021**, *9*, 1821. [CrossRef]
32. Chebbi, M.; Chibani, S.; Paul, J.-F.; Cantrel, L.; Badawi, M. Evaluation of volatile iodine trapping in presence of contaminants: A periodic DFT study on cation exchanged-faujasite. *Microporous Mesoporous Mater.* **2016**, *239*, 111–122. [CrossRef]
33. AbuKhadra, M.R.; Basyouny, M.G.; El-Sherbeeny, A.M.; El-Meligy, M.A.; Elgawad, A.E.E.A. Transesterification of commercial waste cooking oil into biodiesel over innovative alkali trapped zeolite nanocomposite as green and environmental catalysts. *Sustain. Chem. Pharm.* **2020**, *17*, 100289. [CrossRef]
34. Albukhari, S.M.; Salam, M.A.; Abukhadra, M.R. Effective retention of inorganic Selenium ions (Se (VI) and Se (IV)) using novel sodalite structures from muscovite; characterization and mechanism. *J. Taiwan Inst. Chem. Eng.* **2021**, *120*, 116–126. [CrossRef]
35. Fattahi, N.; Triantafyllidis, K.; Luque, R.; Ramazani, A. Zeolite-Based Catalysts: A Valuable Approach toward Ester Bond Formation. *Catalysts* **2019**, *9*, 758. [CrossRef]
36. Ayele, L.; Pérez-Pariente, J.; Chebude, Y.; Díaz, I. Conventional versus alkali fusion synthesis of zeolite A from low grade kaolin. *Appl. Clay Sci.* **2016**, *132–133*, 485–490. [CrossRef]
37. Halász, G.; Szlepák, E.; Szilágyi, E.; Zagyva, A.; Fekete, I. Application of EU Water Framework Directive for monitoring of small water catchment areas in Hungary, II. Preliminary study for establishment of surveillance monitoring system for moderately loaded (rural) and heavily loaded (urban) catchment areas. *Microchem. J.* **2007**, *85*, 72–79. [CrossRef]
38. Altoom, N.; Adlii, A.; Othman, S.I.; Allam, A.A.; Alqhtani, H.A.; Al-Otaibi, F.S.; Abukhadra, M.R. Synthesis and characterization of β-cyclodextrin functionalized zeolite-A as biocompatible carrier for Levofloxacin drug; loading, release, cytotoxicity, and anti-inflammatory studies. *J. Solid State Chem.* **2022**, *312*, 123280. [CrossRef]
39. Sakızcı, M.; Özer, M. The characterization and methane adsorption of Ag-, Cu-, Fe-, and H-exchanged chabazite-rich tuff from Turkey. *Environ. Sci. Pollut. Res.* **2019**, *26*, 16616–16627. [CrossRef]
40. Fu, H.; Yang, Y.; Zhu, R.; Liu, J.; Usman, M.; Chen, Q.; He, H. Superior adsorption of phosphate by ferrihydrite-coated and lanthanum-decorated magnetite. *J. Colloid Interface Sci.* **2018**, *530*, 704–713. [CrossRef]
41. Salehi, S.; Hosseinifard, M. Optimized removal of phosphate and nitrate from aqueous media using zirconium functionalized nanochitosan-graphene oxide composite. *Cellulose* **2020**, *27*, 8859–8883. [CrossRef]
42. Sherlala, A.; Raman, A.; Bello, M.; Buthiyappan, A. Adsorption of arsenic using chitosan magnetic graphene oxide nanocomposite. *J. Environ. Manag.* **2019**, *246*, 547–556. [CrossRef]
43. Huang, Y.; Zeng, X.; Guo, L.; Lan, J.; Zhang, L.; Cao, D. Heavy metal ion removal of wastewater by zeolite-imidazolate frameworks. *Sep. Purif. Technol.* **2018**, *194*, 462–469. [CrossRef]
44. Jasper, E.E.; Ajibola, V.O.; Onwuka, J.C. Nonlinear regression analysis of the sorption of crystal violet and methylene blue from aqueous solutions onto an agro-waste derived activated carbon. *Appl. Water Sci.* **2020**, *10*, 132. [CrossRef]
45. El Qada, E. Kinetic Behavior of the Adsorption of Malachite Green Using Jordanian Diatomite as Adsorbent. *Jordanian J. Eng. Chem. Ind. (JJECI) Res. Pap.* **2020**, *3*, 1–10. [CrossRef]

46. Abukhadra, M.R.; Shemy, M.H.; Khim, J.S.; Ajarem, J.S.; Rabie, A.M.; Abdelrahman, A.A.; Allam, A.A.; Salem, H.M.; Shaban, M.S. Insight into the Adsorption Properties of β-Cyclodextrin/Zeolite-A Structure for Effective Removal of Cd^{2+}, PO_4^{3-}, and Methyl Parathion; Kinetics and Advanced Equilibrium Studies. *J. Inorg. Organomet. Polym. Mater.* **2022**, *32*, 1–15. [CrossRef]
47. Lin, X.; Xie, Y.; Lu, H.; Xin, Y.; Altaf, R.; Zhu, S.; Liu, D. Facile preparation of dual La-Zr modified magnetite adsorbents for efficient and selective phosphorus recovery. *Chem. Eng. J.* **2020**, *413*, 127530. [CrossRef]
48. Huang, Y.; Li, S.; Chen, J.; Zhang, X.; Chen, Y. Adsorption of Pb(II) on mesoporous activated carbons fabricated from water hyacinth using H3PO4 activation: Adsorption capacity, kinetic and isotherm studies. *Appl. Surf. Sci.* **2014**, *293*, 160–168. [CrossRef]
49. Sayed, M.R.; Abukhadra, M.R.; Ahmed, S.A.; Shaban, M.; Javed, U.; Betiha, M.A.; Shim, J.-J.; Rabie, A.M. Synthesis of advanced MgAl-LDH based geopolymer as a potential catalyst in the conversion of waste sunflower oil into biodiesel: Response surface studies. *Fuel* **2020**, *282*, 118865. [CrossRef]
50. Ashraf, M.-T.; AlHammadi, A.A.; El-Sherbeeny, A.M.; Alhammadi, S.; Al Zoubi, W.; Ko, Y.G.; Abukhadra, M.R. Synthesis of cellulose fibers/Zeolite-A nanocomposite as an environmental adsorbent for organic and inorganic selenium ions; Characterization and advanced equilibrium studies. *J. Mol. Liq.* **2022**, *360*, 119573. [CrossRef]
51. Abukhadra, M.R.; Bakry, B.M.; Adlii, A.; Yakout, S.M.; El-Zaidy, M.E. Facile conversion of kaolinite into clay nanotubes (KNTs) of enhanced adsorption properties for toxic heavy metals (Zn2+, Cd2+, Pb2+, and Cr6+) from water. *J. Hazard. Mater.* **2019**, *374*, 296–308. [CrossRef] [PubMed]
52. Giles, C.H.; MacEwan, T.H.; Nakhwa, S.N.; Smith, D. Studies in adsorption. Part XI. A system of classification of solution adsorption isotherms, and its use in diagnosis of adsorption mechanisms and in measurement of specific surface areas of solids. *J. Chem. Soc.* **1960**, *111*, 3973–3993. [CrossRef]
53. Shaban, M.; Abukhadra, M.R.; Shahien, M.G.; Khan, A.A.P. Upgraded modified forms of bituminous coal for the removal of safranin-T dye from aqueous solution. *Environ. Sci. Pollut. Res.* **2017**, *24*, 18135–18151. [CrossRef] [PubMed]
54. Dawodu, F.A.; Akpomie, G.K.; Abuh, M.A. Equilibrium Isotherm Studies on the Batch Sorption of Copper (II) ions from Aqueous Solution unto Nsu Clay. *Int. J. Sci. Eng. Res.* **2012**, *3*, 1–7.
55. Dhaouadi, F.; Sellaoui, L.; Badawi, M.; Reynel-Ávila, H.E.; Mendoza-Castillo, D.I.; Jaime-Leal, J.E.; Bonilla-Petriciolet, A.; Ben Lamine, A. Statistical physics interpretation of the adsorption mechanism of Pb2+, Cd2+ and Ni2+ on chicken feathers. *J. Mol. Liq.* **2020**, *319*, 114168. [CrossRef]
56. Yang, X.; Wang, J.; El-Sherbeeny, A.M.; AlHammadi, A.A.; Park, W.-H.; Abukhadra, M.R. Insight into the adsorption and oxidation activity of a ZnO/piezoelectric quartz core-shell for enhanced decontamination of ibuprofen: Steric, energetic, and oxidation studies. *Chem. Eng. J.* **2021**, *431*, 134312. [CrossRef]
57. Mostafa, M.; El-Meligy, M.A.; Sharaf, M.; Soliman, A.T.; AbuKhadra, M.R. Insight into chitosan/zeolite-A nanocomposite as an advanced carrier for levofloxacin and its anti-inflammatory properties; loading, release, and anti-inflammatory studies. *Int. J. Biol. Macromol.* **2021**, *179*, 206–216. [CrossRef]
58. Seliem, M.K.; Komarneni, S.; Abu Khadra, M.R. Phosphate removal from solution by composite of MCM-41 silica with rice husk: Kinetic and equilibrium studies. *Microporous Mesoporous Mater.* **2015**, *224*, 51–57. [CrossRef]
59. Xie, J.; Wang, Z.; Lu, S.; Wu, D.; Zhang, Z.; Kong, H. Removal and recovery of phosphate from water by lanthanum hydroxide materials. *Chem. Eng. J.* **2014**, *254*, 163–170. [CrossRef]
60. Zhang, G.; Liu, H.; Liu, R.; Qu, J. Removal of phosphate from water by a Fe–Mn binary oxide adsorbent. *J. Colloid Interface Sci.* **2009**, *335*, 168–174. [CrossRef]
61. Yao, Y.; Gao, B.; Inyang, M.; Zimmerman, A.; Cao, X.; Pullammanappallil, P.; Yang, L. Removal of phosphate from aqueous solution by biochar derived from anaerobically digested sugar beet tailings. *J. Hazard. Mater.* **2011**, *190*, 501–507. [CrossRef] [PubMed]
62. Nodeh, H.R.; Sereshti, H.; Afsharian, E.Z.; Nouri, N. Enhanced removal of phosphate and nitrate ions from aqueous media using nanosized lanthanum hydrous doped on magnetic graphene nanocomposite. *J. Environ. Manag.* **2017**, *197*, 265–274. [CrossRef] [PubMed]
63. Das, J.; Patra, B.S.; Baliarsingh, N.; Parida, K.M. Adsorption of phosphate by layered double hydroxides in aqueous solutions. *Appl. Clay Sci.* **2006**, *32*, 252–260. [CrossRef]
64. Zong, E.; Wei, D.; Wan, H.; Zheng, S.; Xu, Z.; Zhu, D. Adsorptive removal of phosphate ions from aqueous solution using zirconia-functionalized graphite oxide. *Chem. Eng. J.* **2013**, *221*, 193–203. [CrossRef]
65. Alshameri, A.; Yan, C.; Lei, X. Enhancement of phosphate removal from water by TiO_2/Yemeni natural zeolite: Preparation, characterization and thermodynamic. *Microporous Mesoporous Mater.* **2014**, *196*, 145–157. [CrossRef]
66. Sakulpaisan, S.; Vongsetskul, T.; Reamouppaturm, S.; Luangkachao, J.; Tantirungrotechai, J.; Tangboriboonrat, P. Titania-functionalized graphene oxide for an efficient adsorptive removal of phosphate ions. *J. Environ. Manag.* **2016**, *167*, 99–104. [CrossRef]
67. Su, Y.; Cui, H.; Li, Q.; Gao, S.; Shang, J.K. Strong adsorption of phosphate by amorphous zirconium oxide nanoparticles. *Water Res.* **2013**, *47*, 5018–5026. [CrossRef]
68. Hamdi, N.; Srasra, E. Removal of phosphate ions from aqueous solution using Tunisian clays minerals and synthetic zeolite. *J. Environ. Sci.* **2012**, *24*, 617–623. [CrossRef]

69. Lin, J.; Zhan, Y.; Wang, H.; Chu, M.; Wang, C.; He, Y.; Wang, X. Effect of calcium ion on phosphate adsorption onto hydrous zirconium oxide. *Chem. Eng. J.* **2016**, *309*, 118–129. [CrossRef]
70. Shi, W.; Fu, Y.; Jiang, W.; Ye, Y.; Kang, J.; Liu, D.; Ren, Y.; Li, D.; Luo, C.; Xu, Z. Enhanced phosphate removal by zeolite loaded with Mg–Al–La ternary (hydr)oxides from aqueous solutions: Performance and mechanism. *Chem. Eng. J.* **2018**, *357*, 33–44. [CrossRef]

Disclaimer/Publisher's Note: The statements, opinions and data contained in all publications are solely those of the individual author(s) and contributor(s) and not of MDPI and/or the editor(s). MDPI and/or the editor(s) disclaim responsibility for any injury to people or property resulting from any ideas, methods, instructions or products referred to in the content.